35th Annual International Conference of the IEEE EMBS
Osaka, Japan, 3 - 7 July, 2013

Localization of brachytherapy seeds in MRI by deconvolution

Ying Dong[1], Zheng Chang[2], Gregory Whitehead[1] and Jim Ji[1]

[1]Department of Electrical and Computer Engineering, Texas A&M University
[2]Department of Radiation Oncology, Duke University

Abstract—**MRI has the potential to be used as a preferred imaging method for brachytherapy during the seed insertion and post-surgery evaluation. However, the brachytherapy seeds usually appear dark in the MRI magnitude images. Previously, we have developed a method based on susceptibility mapping to generate positive contrast of the seeds, which allows improved seed localization. In this paper, we propose a new method to localize the seeds by deconvolution using a seed kernel (i.e. the calculated magnetic field surrounding a seed). The deconvolution is solved using a regularized L_1 minimization. Results from simulated and experimental data sets show that the seeds can be identified and localized using the proposed method more precisely.**

I. Introduction

Brachytherapy, by directly inserting radioactive material into the cancer tissues, is an effective way to kill malignant cells by providing highly localized radiations[1]. Visual assistance is needed to monitor and evaluate during and after the operation. Conventionally preferred modality for this application is ultrasound imaging due to its fast speed and low cost. With the ability to provide high resolution and soft tissue contrast, MRI has been explored as an alternative, more powerful imaging modality in such procedures [2].

In MRI, brachytherapy seeds normally appear dark due to the rapid dephasing caused by the high susceptibility of the metallic shell. Therefore, it is difficult to differentiate the seeds from other dark structures, such as the cavities/voids in the tissue. This can lead to inaccurate quantification of radiation doses. Our group has proposed a method based on susceptibility map to provide the positive contrast of brachytherapy seeds [3]. In the method, susceptibility is calculated by deconvoluting the magnetic field map with a dipole kernel. However, in practice, susceptibility mapping may not be consistent across slices. Moreover, the susceptibility map does not directly provide location information.

In this paper, we extend on the method in [3] to provide a more precise and robust brachytherapy seed localization using MRI. In the proposed method, we calculated the field map of a nominal seed, which is then used as the deconvolution kernel. The deconvolution is solved using a regularized L_1 minimization, which iteratively extracts the location map of the seeds from the magnetic field measured by MRI. Computer simulations and phantom experiments on a 4.7 Tesla scanner are used to demonstrate the feasibility of the method. Results show the proposed method can provide more precise localization.

Ying Dong, Gregory Whitehead and Jim Ji are with the Department of Electrical and Computer Engineering, Texas A&M University, College Station, TX 77843-3128 USA (corresponding author: Jim Ji, phone: 979-458-1468; fax: 979-845-6259; e-mail: jimji@tamu.edu).

II. Theory and Method

The magnetic field caused by a magnetically susceptible object can be modeled as a linear sum of the fields from its finite elements. Therefore, the magnetic field $\Delta\mathbf{B}(\mathbf{r})$ surrounding an object can be modeled as the convolution of the spatial susceptibility distribution of the object(s) $\chi(\mathbf{r})$ and a dipole kernel [4]:

$$\Delta\mathbf{B}(\mathbf{r}) = \boldsymbol{\kappa}_d(\mathbf{r}) \otimes \chi(\mathbf{r}) \tag{1}$$

where $\boldsymbol{\kappa}_d(\mathbf{r}) = \dfrac{3\cos^2(\theta_\mathbf{r}) - 1}{4\pi|\mathbf{r}|^3}$ is thje dipole kernel where $\theta_\mathbf{r}$ is the angle between $\mathbf{r}$ and z axis [5]. Once $\Delta\mathbf{B}(\mathbf{r})$ is measured, susceptibility distribution can be in principle obtained by dipole kernel deconvolution.

In this paper, we extend the above model to incorporate the shape and susceptibility of the brachytherapy seeds. Specifically let

$$\begin{aligned}\Delta\mathbf{B}(\mathbf{r}) &= \boldsymbol{\kappa}_d(\mathbf{r}) \otimes \chi(\mathbf{r}) \\ &= \boldsymbol{\kappa}_d(\mathbf{r}) \otimes \mathbf{S}(\mathbf{r}) \otimes \mathbf{L}(\mathbf{r}) + \boldsymbol{\kappa}_d(\mathbf{r}) \otimes \chi_b(\mathbf{r}) \\ &= \boldsymbol{\kappa}_s(\mathbf{r}) \otimes \mathbf{L}(\mathbf{r}) + \boldsymbol{\kappa}_d(\mathbf{r}) \otimes \chi_b(\mathbf{r})\end{aligned} \tag{2}$$

where $\boldsymbol{\kappa}_s(\mathbf{r}) = \boldsymbol{\kappa}_d(\mathbf{r}) \otimes \mathbf{S}(\mathbf{r})$ is the seed kernel where $\mathbf{S}(\mathbf{r})$ is the seed shape function whose value is the relative susceptibility of the material at $\mathbf{r}$. $\mathbf{L}(\mathbf{r})$ is a union of Dirac delta functions indicating the seed locations. $\chi_b(\mathbf{r})$ is the susceptibility function of the background. Therefore, by deconvolution of the field map with the seed kernel, we can recover the locations of the seeds, i.e., $\mathbf{L}(\mathbf{r})$. Note that the second term in Eq. (2) is expected to be diffused or reduced after

deconvolution when the susceptibility of the background tissues does not match with that of a seed.

The seed kernel is calculated by the integral of the dipole kernel over the whole seed. For example, STM 1251 I-125 seeds have a cylindrical titanium with a length of l =4.55mm and diameter of d =0.81mm, and inner aluminum wire with length of l =3.81mm and diameter of d =0.51mm [6]. Therefore

$$\boldsymbol{\kappa}_s(\mathbf{r})=\int_{\mathbf{r}'\neq\mathbf{r}}\frac{3\cos^2(\theta_{\mathbf{r}-\mathbf{r}'})-1}{4\pi\left|\mathbf{r}-\mathbf{r}'\right|^3}\cdot\mathbf{S}(\mathbf{r})d^3\mathbf{r}'=\boldsymbol{\kappa}_d(\mathbf{r})\otimes\mathbf{S}(\mathbf{r}) \quad (3)$$

where $\mathbf{r}'=(x',y',z')$ is a vector of a point inside the seed. This integral can also be considered as the convolution of the dipole kernel with the shape of the seed.

The integral depends on the orientation of the seed, as shown in Fig. 1. For example when the seed is orthogonal to the magnetic field, the integral can be calculated by

$$\boldsymbol{\kappa}_s=\int_{-\frac{l}{2}}^{\frac{l}{2}}\int_{-\frac{d}{2}}^{\frac{d}{2}}\int_{-\sqrt{(\frac{d}{2})^2-z'^2}}^{\sqrt{(\frac{d}{2})^2-z'^2}}\frac{3\cos^2(\theta_{\mathbf{r}-\mathbf{r}'})-1}{4\pi\left|\mathbf{r}-\mathbf{r}'\right|^3}\cdot\mathbf{S}(\mathbf{r})dx'dz'dy' \quad (4)$$

where $r=\left|\mathbf{r}-\mathbf{r}'\right|=\sqrt{(x-x')^2+(y-y')^2+(z-z')^2}$, and

$$\cos\theta_{\mathbf{r}-\mathbf{r}'}=\frac{\mathbf{u}_z\cdot(\mathbf{r}-\mathbf{r}')}{\left|\mathbf{u}_z\right|\left|\mathbf{r}-\mathbf{r}'\right|}=\frac{z-z'}{r}.$$

Numerically, this integral can be evaluated on the rectilinear sampling matrix by using the finite summation approximation in the spatial domain, or by applying convolution theorem in Fourier domain.

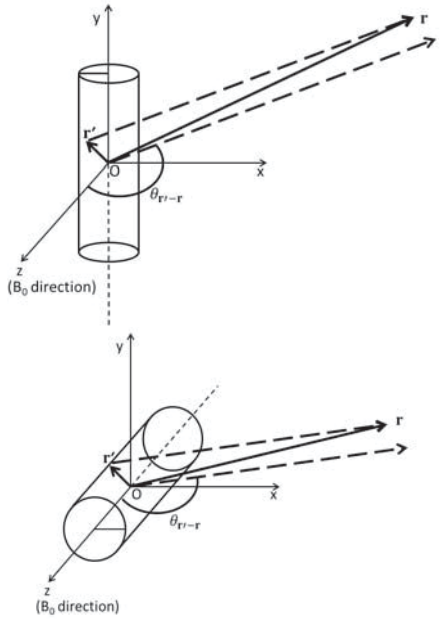

Fig.1 Illustration of seeds at different orientations in the magnet. The seed is (a) orthogonal or (b) parallel to the external magnetic field (B_0).

1. Deconvolution using regularized L_1 minimization

Based on Eq. (2), the measured off-resonance field can be expressed as a matrix operation,

$$\boldsymbol{\psi}=\boldsymbol{\kappa}_s\otimes\mathbf{E}=\mathbf{KE} \quad (5)$$

where $\boldsymbol{\psi}$ is the measure magnetic field map, $\mathbf{K}$ is the discretized seed kernel convolution matrix,and $\mathbf{E}$ is the discretized location map. In practice, the field map can be obtained from two or more images acquired at shifted echo times [7].

In principle, the convolution in spatial domain is the same as the point-wise multiplication in the frequency domain. Therefore, $\mathcal{F}(\boldsymbol{\psi})=\mathcal{F}(\boldsymbol{\kappa}_s)\cdot\mathcal{F}(\mathbf{E})$, where $\mathcal{F}$ is the Fourier transform. So deconvolution can be performed by $\mathbf{E}=\mathcal{F}^{-1}(\mathcal{F}(\boldsymbol{\psi})\cdot\frac{1}{\mathcal{F}(\boldsymbol{\kappa}_s)})$. However, such direct deconvolution method is not practical because $\mathcal{F}(\boldsymbol{\kappa}_s)$ contains zeros. In this paper, we solve $\mathbf{E}$ by a regularized L_1 minimization. This is because the number of the brachytherapy seeds is small, and the location map can be considered sparse. Specifically, the location map is achieved from

$$\arg\min_{\mathbf{E}}\left\|\mathbf{MGE}\right\|_1 \quad \text{subject to } \left\|\mathbf{A}(\mathbf{KE}-\boldsymbol{\psi})\right\|_2\le\varepsilon \quad (6)$$

where $\mathbf{G}$ is the first order gradient operator , $\mathbf{M}$ is the mask, $\mathbf{A}$ is the point-wise weight which is proportional to the image magnitude, and ε is a small constant related to the noise level. The masking matrix $\mathbf{M}$ is obtained by thresholding the magnitude images. It normally has the same shape as the background tissue, masking out the rough location of the seeds.

After rewriting Eq.(6) into a Lagrangian form and some mathematical manipulation, the L_1 minimization problem can be turned to [5, 7, 8].

$$\min_{\mathbf{E},\lambda} f(\mathbf{E},\lambda)=\left\|\mathbf{A}(\mathbf{KE}-\boldsymbol{\psi})\right\|_2^2+\lambda\left\|\mathbf{MGE}\right\|_1 \quad (7)$$

The first term minimizes the difference between calculation and the acquired data, and the second term promotes the sparsity. To solve Eq. (7), the first order derivative with respect to $\boldsymbol{\chi}$ is set to be 0 such that

$$\frac{\partial f}{\partial\mathbf{E}}=2\mathbf{K}^H\mathbf{A}^H(\mathbf{A}(\mathbf{KE}-\boldsymbol{\psi}))+\lambda\nabla\left\|\mathbf{MGE}\right\|_1=0 \quad (8)$$

where ^{H} is the conjugate operator. $\left\|\mathbf{MGE}\right\|_1$ is not continuous at 0, so a small regularization number is added to make it continuous and differentiable [8]. So Eq. (8) cecomes

$$\frac{\partial f}{\partial\mathbf{E}}\approx 2\mathbf{K}^H\mathbf{A}^H(\mathbf{A}(\mathbf{KE}-\boldsymbol{\psi}))+\lambda\mathbf{G}^H\mathbf{M}^H\mathbf{W}^{-1}\mathbf{MGE} \quad (9)$$

where $\mathbf{W}$ is a diagonal matrix and $\omega_k=\sqrt{(\mathbf{MGE})_k^*(\mathbf{MGE})_k+\mu}$ is the diagonal elements, where μ is a number much smaller than sampled data. In this paper, μ is experimentally set to 10^{-15}.

Eq. (9) is solved iteratively using a nonlinear conjugate gradient method [8]. The iteration stops either when the gradient is smaller than a preset lower bound or when it reaches the maximum iterations allowed.

2. Data simulation and experimental acquisition

A computer simulation was first used to validate the proposed method. The object in the simulation is block of tissue with two seeds inserted. The susceptibility of the

rectangular block was set to be 9 ppm, and that of the seeds was 100 ppm. The image matrix size in the simulation was 128×128×7, the FOV was set to 60×60×10.5mm^3. These parameters were chosen so that they are similar to one set of the experimental data (described below). Two seeds were placed in a uniform-susceptibility rectangular block. The seeds were set to be orthogonal to the main magnetic field. The field map was calculated by convoluting the dipole kernel with the susceptibility distribution. White noise were added directly to the field map (yielding SNR = 20/40 dB). Direct deconvolution method using the seed kernel and the proposed method (λ=10^{-3}) were both applied to recover the location of the seeds.

In addition, two experimental data sets were acquired on a 4.7 Tesla, 33-cm bore scanner. In both experiments, three STM 1251 dummy seeds (seeds without radioactive material) were imaged with a spin-echo sequence with shifted 180° RF pulse. In the first experiment, a gelatin phantom doped with copper sulfate with the inserted seeds was imaged. Two seeds were placed in parallel to the main magnetic field. The matrix size was 128×128×7. The FOV was 80×80mm^2. The slice thickness was 1mm, and slice gap was 0.5mm. The TR was 2s, and the TE was 30ms. There sets of images were acquired, with 180° RF pulse being shifted by T_{shift} =[-0.3, 0, 0.3]ms respectively. The field map was calculated by a linear fitting algorithm according to $\psi = \frac{\Delta\varphi}{2\gamma B_0 T_{shift}}$, where $\Delta\varphi$ is the phase change between the acquisitions.

In the second experiment, the acquisition parameters were identical to the first one except that the FOV is 60×60mm^2. However, phantom material used was beef instead of gelatin. In this experiment, three seeds were placed orthogonal to the main magnetic field.

All data processing and deconvolution procedures were performed offline using Matlab (Math Works, Natick, MA). The computer has an Intel® Core™ 2 Duo CPU T8300 @2.40GHz, 2GB RAM, and Windows 7 Ultimate operating system. Multiple regularization parameters were tested and visually compared to choose the best results.

III. Results

Fig. 2 shows the simulated field maps and the seed localization results using the direct deconvolution method and the proposed method. The left column has SNR = 40dB. The location of the seed using both the direct method and the proposed method can be clearly seen, even slight degradation is shown in the background. The right column has SNR = 20dB. The background is corrupted with the direct deconvolution method, which makes it difficult to identify the seeds. With the proposed method, the locations of the seeds are correctly recovered and the background is smooth in both cases. The proposed method broke at higher noise level (with SNR~5dB). In all cases, the computation time is around 140 seconds.

Fig. 3 shows the representative phase images in the center slice for the first experimental data set. No obvious phase difference between the seeds and the gelatin is observed when T_{shift} = 0ms. This is because with the spin echo sequence the phase caused by field inhomogeneity is reversed by the 180º pulse. But when the 180° RF pulse is shifted, the spins cannot get refocused during the acquisition window. The field map shows gradual phase changes around the seeds. As shown, the filed map indicates the location of the seeds. However, one cannot accurately locate the seeds just from the field map because it is diffused. The results using the proposed method in Fig. 3(d) show more localized seed position.

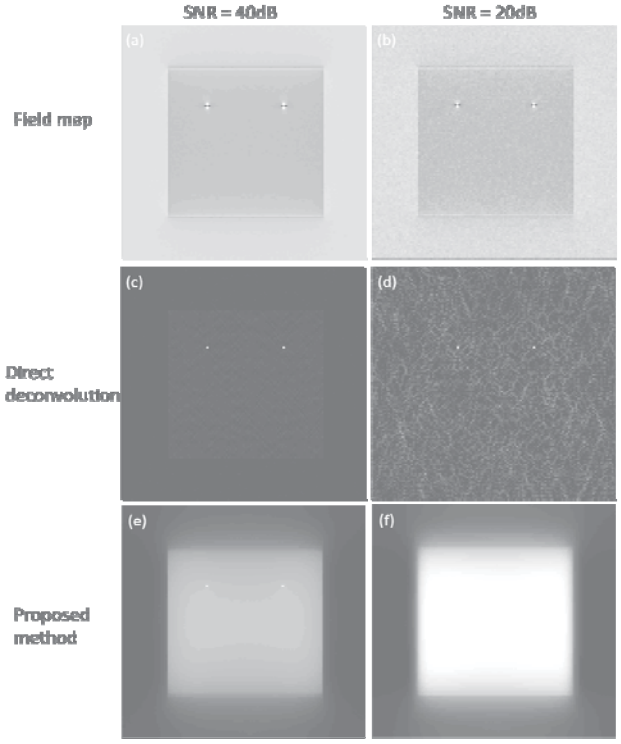

Fig.2 Seed localization using the direct deconvolution and the proposed method in the simulated study.

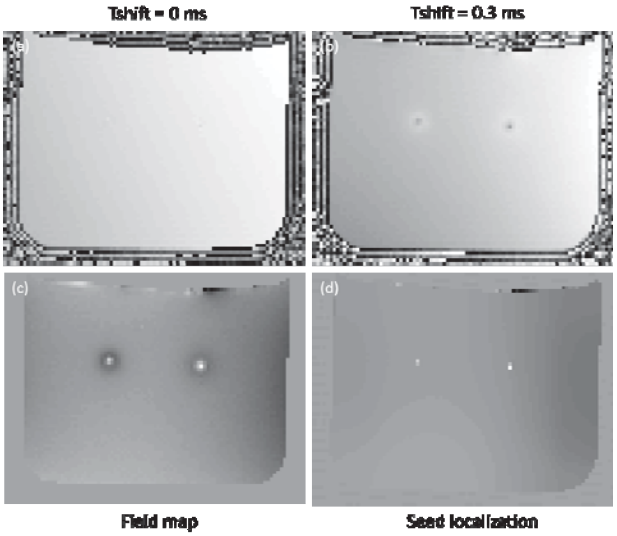

Fig.3 The representative phase images in the center slice (slice 4) for the first experimental data set with (a) T_{shift} = 0 and (b) 0.3ms. (c) The calculated field map and (d) localization of the seeds using the proposed method. Images are cropped for better visualization.

Fig. 4 shows the representative phase images of the second experimental data set. As beef is less homogeneous than the gelatin phantom, this represents a more challenging scenario. Note that the field map is much more inhomogeneous and noisier. As a result, the seeds are more difficult to distinguish from the tissues in this experiment. Direct Fourier deconvolution on this dataset yields no meaningful result (which is not shown). The proposed method produced a highly localized, clear representation of the seed position, as shown in Fig. 4(d).

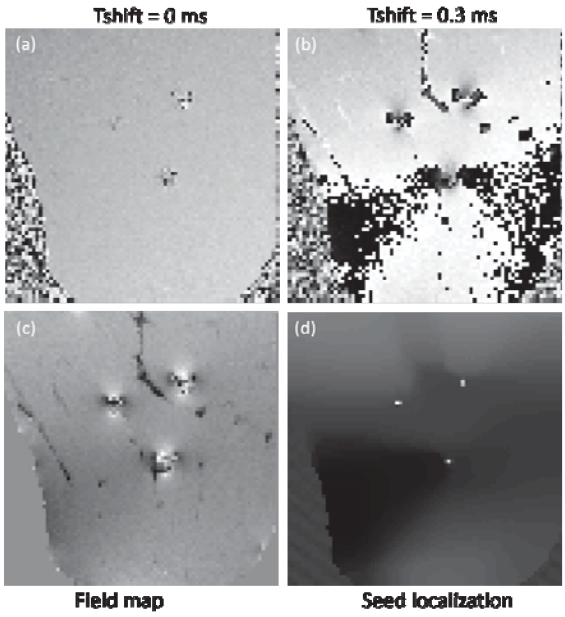

Fig.4 The representative phase images of the second experimental data set in the center slice (slice 4) with (a) $T_{shift} = 0$ and (b) 0.3ms. (c) The calculated field map and (d) localization of the seeds using the proposed method. Images are cropped for better visualization.

IV. Discussion

The simulated and experimental results have clearly demonstrated the feasibility of the proposed method. However, there are several expected limitations. First, due to the field inhomogeneous, noise and large field map variance, the bright spots in the result location map may present in more than one pixel and/or more than one slice. In that case, there will still be some ambiguity on the seed location, which may need further processing

Another potential difficulty is that the seeds may be put in various orientations. In the experiments, we show the feasibility when the seeds are parallel or orthogonal to the magnetic field. In clinical practice, the seeds are inserted using guide and therefore will be in the same direction. However, post-surgery tissue movement and deformation can change the seed orientation. To make the proposed method capable of handling more general cases, the algorithm needs to add an additional steps to search in the range of all possible orientations.

V. Conclusion

In this paper, we developed a method to localize brachytherapy seeds by a seed field deconvolution. The deconvolution was solved using a regularized L1 minimization, which iteratively extracted the location map of the seeds from the magnetic field measured by MRI. A set of simulated data and two sets of the experimental data were used to demonstrate the feasibility of the method. Results showed the proposed deconvolution using the seed kernel is more capable than the conventional dipole kernel deconvolution. Notably, only the structure with the same shape as the seed will result in high spot in the location map produced. Other susceptible tissues, which are easier to be confused with the seeds, become diffused. This allows more accurate and precise seed localization, which is expected to improve the dose accuracy and reliability of brachytherapy.

Acknowledgement

This work was supported in part by the National Science Foundation under award number 0748180. Any opinions, findings and conclusions or recommendations expressed in this material are those of the authors and do not necessarily reflect those of the National Science Foundation.

References

[1] A. V. D'Amico, *et al.*, "Real-time magnetic resonance image-guided interstitial brachytherapy in the treatment of select patients with clinically localized prostate cancer," *International Journal of Radiation Oncology* Biology* Physics,* vol. 42, pp. 507-515, 1998.

[2] R. C. Susil, *et al.*, "System for prostate brachytherapy and biopsy in a standard 1.5 T MRI scanner," *Magnetic Resonance in Medicine,* vol. 52, pp. 683-687, 2004.

[3] D. Ying and J. Jim, "Positive contrast MRI of prostate brachytherapy seeds by susceptibility mapping," in *Engineering in Medicine and Biology Society (EMBC), 2012 Annual International Conference of the IEEE*, 2012, pp. 392-395.

[4] J. D. Jackson and R. F. Fox, "Classical electrodynamics," *American Journal of Physics,* vol. 67, p. 841, 1999.

[5] J. Liu, *et al.*, "Morphology enabled dipole inversion for quantitative susceptibility mapping using structural consistency between the magnitude image and the susceptibility map," *Neuroimage,* 2011.

[6] A. S. Kirov and J. F. Williamson, "Monte-Carlo-aided dosimetry of the Source Tech Medical Model STM1251 I-125 interstitial brachytherapy source," *Med. Phys.,* vol. 28, pp. 764-772, 2001.

[7] B. Kressler, *et al.*, "Nonlinear regularization for per voxel estimation of magnetic susceptibility distributions from MRI field maps," *Medical Imaging, IEEE Transactions on,* vol. 29, pp. 273-281, 2010.

[8] M. Lustig, *et al.*, "Sparse MRI: The application of compressed sensing for rapid MR imaging," *Magnetic Resonance in Medicine,* vol. 58, pp. 1182-1195, 2007.